Heliyon 10 (2024) e29260

Contents lists available at ScienceDirect

Heliyon

journal homepage: www.cell.com/heliyon

Research article

Application of bolus tracking: The effect of ROI positions on the images quality of cervicocerebral CT angiography

Huiming Wu [a], Jianhua Wang [a], Maodong Zhou [a], Yajie Wang [a], Can Cui [a], Changsheng Zhou [b], Xiao Chen [a,*], Zhongqiu Wang [a,**]

[a] Department of Radiology, The Affiliated Hospital of Nanjing University of Chinese Medicine, 155 Hanzhong road, Nanjing, 210029, China
[b] Department of Radiology, Jinling Hospital Nanjing University, 305 Zhongshan East road, Nanjing, 210029, China

ARTICLE INFO

Keywords:
Bolus tracking
CT angiography
Head and neck
Region of interest

ABSTRACT

Background: Cervicocerebral CT angiography (CTA) using the bolus tracking technique has been widely used for the assessment of cerebrovascular diseases. Regions of interest (ROI) can be placed in the descending aorta, ascending aorta, and the aortic arch. However, no study has compared the arteries and veins display when when the region of interest (ROI) is placed at different sites. In this study, we showed the impact of ROI positions on the image quality of cervicocerebral CTA.

Methods: Two hundred and seventy patients who underwent cervicocerebral CTA with bolus tracking technique were randomly divided into three groups based on the position of the ROI placement: ascending aorta (Group 1, n = 90), aortic arch (Group 2, n = 90), and descending aorta (Group 3, n = 90). The scanning parameters and contrast agent injection protocols were consistent across all groups. Three observers independently assessed the objective image quality, while two observers jointly assessed the subjective image quality using a grade scale: poor (grade 1), average (grade 2), good (grade 3), and excellent (grade 4). The differences in intravascular CT values, signal-to-noise ratio (SNR), contrast-to-noise ratio (CNR), AVCR (arterial venous contrast ratio), and subjective image quality scores were compared among the three groups.

Results: The CT values of the intracranial veins (superior sagittal sinus, ethmoid sinus and great cerebral vein) in group 1 were significantly lower than those in group 3 ($p < 0.001$). However, no significant differences were observed in CT values, SNR and CNR in the internal carotid artery and middle cerebral artery among the three groups. The proportion of images with grade 4 was significantly higher in group 1 than group 2 and 3 (41.1% vs 15.6% and 13.3%, $p < 0.001$). The proportion of images with grade 1 was significantly lower in group 1 than group 2 and 3 (1.1% vs 6.6% and 17.8%, $p < 0.001$).

Conclusion: The ROI positions for cervicocerebral CTA did not affect the arterial image quality, but venous structures imaging was affected when the ROI was placed in the ascending aorta.

* Corresponding author. The Affiliated Hospital of Nanjing University of Chinese Medicine, China.
** Corresponding author. The Affiliated Hospital of Nanjing University of Chinese Medicine, China.
E-mail addresses: fsyy00597@njucm.edu.cn (X. Chen), zhqwang002@126.com (Z. Wang).

https://doi.org/10.1016/j.heliyon.2024.e29260
Received 4 August 2023; Received in revised form 28 March 2024; Accepted 3 April 2024
Available online 4 April 2024

1. Introduction

Computed tomography angiography (CTA) has been widely used for cardiovascular and cerebrovascular diseases. In CT angiography, scan timing is crucial to achieve the good image quality. Currently, bolus tracking is the most frequently utilized angiographic technique in clinical practice [1]. There is an additional delay time after the regions of interest (ROI) reaching the trigger threshold within the monitoring level, depending on the hardware configuration of the various devices and the time of the scanning bed movement [2–4]. A prolonged delay time may lead to missing the peak enhancement or obvious venous noise.

Cervicocerebral CTA is one of the most important imaging examination for detecting vascular lesions in the head and neck [5–7]. Excellent CTA imaging of the head and neck requires sufficient artery enhancement and minimal venous overlay [8–11]. The precise scanning time is critical. The delayed scans after the threshold triggering make the ROI positions a significant factor for bolus tracking technique. The main ROI sites that were commonly used in clinical practice are the aortic arch and the descending aorta [12–14]. According to the pathway of blood flow, the ascending aorta may have priority over the other two sites for enhancement. Theoretically, when a uniform trigger threshold is set, the ascending aorta has a certain probability of triggering the scan earlier than the other two sites, which corresponds to a shorter additional delay time. Consequently, the venous structures may not be adequately opacified on CTA images. However, few studies have focused on placing ROI in the ascending aorta for cervicocerebral CTA. The recent American College of Radiology (ACR) guideline for cervicocerebral CTA indicated that visible and adequately opacified veins should be commented on when appropriate [15]. However, no study has compared the display of arteries and veins when the ROIs are placed at the ascending aorta, the aortic arch, and the descending aorta. In this study, we showed the image quality in the head and neck CTA with the bolus tracking technique with the ROI placed at ascending aorta, the aortic arch, and the descending aorta, respectively.

2. Materials and methods

2.1. Study participants

The Institutional Review Board of the Affiliated Hospital of Nanjing University of Chinese Medicine (2021NL-157-01, Oct 2021) approved this prospective study and written informed consent was obtained from all participants. During the study Declaration of Helsinki was followed. Four hundred and twelve patients who were suspected for cerebrovascular diseases during February–June 2022 were recruited. The exclusion criteria were as follows: weight >100 kg; known previous allergy to iodine contrast agent; severe renal impairment; pregnancy or lactation; moyamoya disease, arteriovenous malformation, intracranial vascular occlusion; pacemaker fitted; left upper limb buried indwelling needle; injection flow rate <5 mL/s due to patient's vasculature; contrast reflux into the internal jugular vein. One hundred and forty two were excluded. Finally, two hundred and seventy subjects were randomly divided into three groups. They underwent cervicocerebral CTA using the bolus tracking technique. The ROIs were placed at the ascending

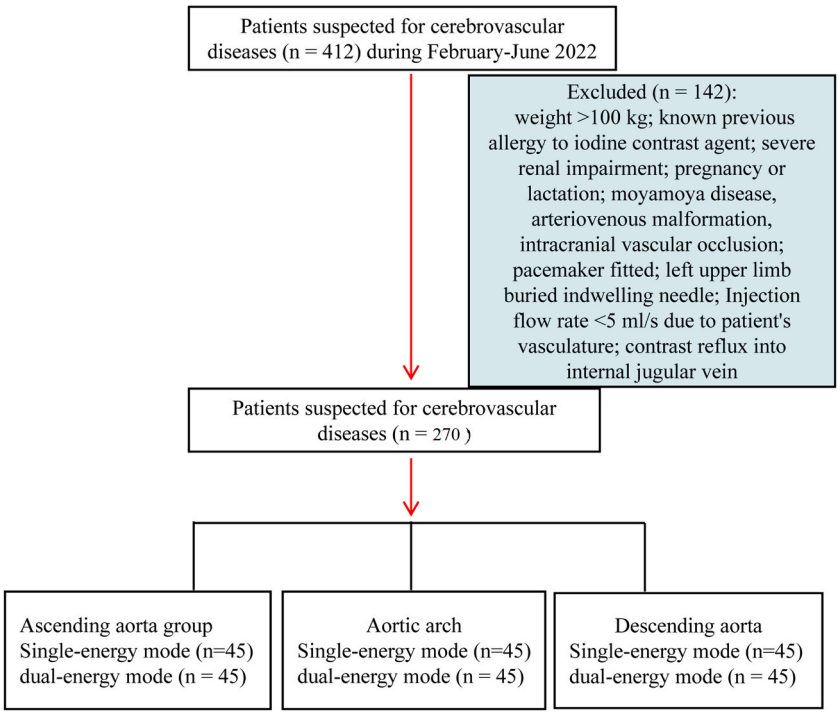

Fig. 1. Flowchart of study. 270 subjects suspected for cervicocerebral artery diseases were randomly divided into three groups.

aorta, aortic arch, and descending aorta, respectively. There were 90 subjects in each groups, with 45 undergoing CTA in the single-energy mode and 45 in the dual-energy mode. The flowchart is shown in Fig. 1.

2.2. Bolus tracking technique

The ROI was placed at the tracheal bifurcation in the ascending aorta (Fig. 2A), aortic arch (Fig. 2B) and descending aorta (Fig. 2C). The ascending aorta and the descending aorta are monitored at the level of the tracheal bifurcation and the aortic arch is monitored at the level the upper and lower aortic arch wall edges (Fig. 2D). The ROI was placed in the center of the vessel and the its area was accounted for approximately 1/3 to 1/2 of the lumen. The trigger threshold was set at 100 Hounsfield unit (HU) for single-energy mode and dual-energy mode. Automated scanning software (SmartPrep; GE Healthcare) was used in our study.

2.3. CT scanning protocol

All examinations were conducted using a 256-row Revolution CT (GE Healthcare). The scan parameters were the same for the subjects who underwent scans using the same modality. Single energy mode: tube voltage 120 kV, smart tube current 300–450 mA, Noise Index, 11. Dual energy mode: tube voltage 80/140 kV; tube current 365 mA; GSI Image Type, Monochromatic 70 keV [16]. The rest of the scanning and reconstruction parameters were the same for both modes. Primary settings: Rotation Time, 0.50 s; Detector Coverage, 80 mm; Pitch, 0.992:1. Reconstruction settings: Thickness and Interval, 0.625 mm; reconstruction type, standard; Reconstruction mode, Helical Plus; Image Reconstruction, 70% ASiR; window/level, 700/50. The scanning parameters are listed in Table 1. The contrast agent injection protocol was the same in all three groups. Briefly, a 20 G indwelling needle was placed in the right upper limb. 30 mL of 0.9% saline was injected using a high-pressure syringe (Missouri-XD-2061-TOUCH; Ulrich). After the start of the examination, 35 mL of non-ionic iodine contrast agent (Omnipaque, 350 mg I/mL, GE Healthcare) was injected at a flow rate of 5 mL/s, followed by 40 mL of saline. Diagnostic CT scanning was initiated with an additional delay of 2.2 s after the bolus-tracking technique program detected the attenuation trigger.

2.4. Objective image quality

Images were sent to Advantage Workstation 4.7 (GE Healthcare) and evaluated by three observers who were unaware of the scan protocols (ZMD with 7 years experience in neurovascular imaging; CC and WYJ with 5 years experience in neurovascular imaging). The CT attenuation was measured in the following vessels: the aortic arch, internal carotid artery (ICA) (bifurcation level), middle cerebral artery (MCA) (M1 segment), superior sagittal sinus (SSS) (cranial parietal level), vein of Galen, and sigmoid sinus (healthy side). The ROI was placed within the target vessel, while avoiding vessel walls, the calcifications, and thrombi. The CT and SD values of the sternocleidomastoid muscle at the ICA bifurcation were also measured to calculate the signal-to-noise ratio (SNR) and contrast-to-noise ratio (CNR) of ICA. Similarly, SNR and CNR of MCA were also calculated. The formula was as follows: $SNR = HUvessel/SDmuscle$; $CNR_{ICA} = (HUvessel - HUmuscle)/SDmuscle$; $CNR_{MCA} = (HUvessel - HUcentrum\ semiovale)/SDmuscle$.

2.5. Subjective image quality

Subjective image quality was assessed by two observers who were blinded to the grouping and imaging procedures (WHM with 12 years experience in cardiovascular imaging; WJH with 15 years in cardiovascular diagnostic). The quality of intracranial vein images was evaluated using axial thin-slab maximum intensity projection (MIP) with a thickness of 20 mm. Images were categorized into four grades: poor (grade 1), adequate arterial imaging with obvious venous structure and it was difficult to distinguish between arteries and veins (Fig. 3A); average (grade 2), adequate arterial imaging with moderate venous enhancement but it was easy to distinguish between arteries and veins (Fig. 3B); good (grade 3), adequate arterial imaging with mild venous enhancement (Fig. 3C); and excellent (grade 4), adequate arterial imaging and no significant venous structure imaging (Fig. 3D). Prior to analyzing the images, both

Fig. 2. Schematic diagram of the monitoring levels. **(A)** region of interest (ROI) was placed in the ascending aorta (red circle); **(B)** ROI was placed in the aortic arch (red circle); **(C)** ROI was placed in the descending aorta (red circle); **(D)** The ascending aorta and the descending aorta are monitored at the level of the tracheal bifurcation (yellow dashed line) and the aortic arch is monitored at the level the upper and lower aortic arch wall edges (red solid line). (For interpretation of the references to colour in this figure legend, the reader is referred to the Web version of this article.)

Table 1
Scanning parameters for single-energy and dual-energy.

	Single-Energy	Dual-Energy
Tube voltage (kVp)	120	80/140
Tube current (mA)	300–450	365
Rotation time (sec)	0.5	0.5
Detector coverage (mm)	80	80
Pitch	0.992:1	0.992:1
Noise index (HU)	11	None
Thickness/interval (mm)	0.625/0.625	0.625/0.625
Recon type	Standard	Standard
Image reconstruction	ASiR-V 70%	ASiR-V 70%
GSI image type	None	Monochromatic 70 keV
Trigger threshold (HU)	100	100

Note.-ASiR = adaptive statistical iterative reconstruction.

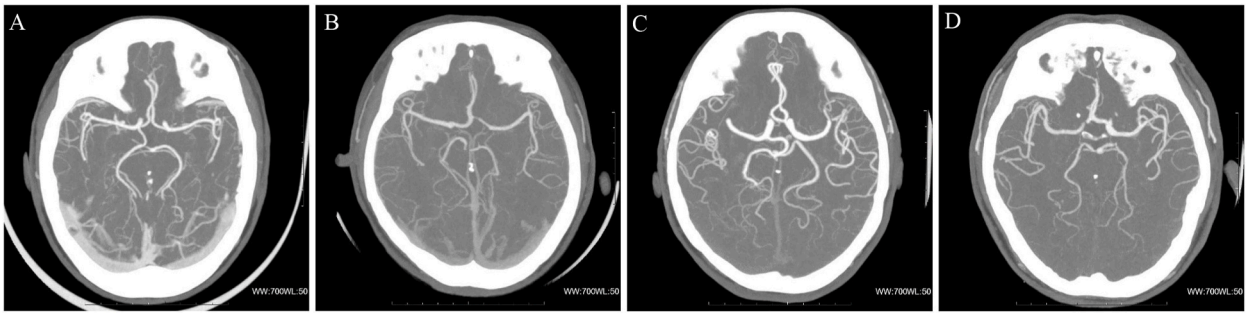

Fig. 3. The illustration of subjective image quality. (a) poor (Grade 1), poor with severe venous contamination and venous enhancement similar to that of the artery; (b) average (Grade 2), poor with moderate venous enhancement and less venous enhancement than the artery, easy to distinguish between arteries and veins; (c) good (Grade 3), good with mild venous enhancement and much less venous enhancement than the artery; and (d) excellent (Grade 4), excellent with significant arterial enhancement and no significant venous contamination.

observers received training sessions to become familiar with the grading system. Disagreements among the observers were resolved thorough the joint reading procedure to determine the final grading.

2.6. Statistical analysis

SPSS (version 26) was used for data management and statistical analysis. The Shapiro-Wilk test was used to assess the normal distribution of continuous data. Quantitative data with normal or near-normal distribution were presented as mean ± standard

Table 2
Study participant demographics and radiation dose estimates.

	Single-Energy				Dual-Energy			
Variables	Ascending aorta	Aortic arch	Descending aorta	*P* Value	Ascending aorta	Aortic arch	Descending aorta	*P* Value
No. of participants	45	45	45		45	45	45	
Age (y)[a]	64 ± 12	65 ± 10	66 ± 10	>0.05	63 ± 10	65 ± 11	62 ± 14	>0.05
Sex								
Male	20 (44)	19 (42)	15 (33)	>0.05	23 (51)	25 (56)	17 (38)	>0.05
Female	25 (56)	26 (58)	30 (67)		22 (49)	20 (44)	28 (62)	
Weight (kg)[a]	66.6 ± 9.7	64.5 ± 10	66 ± 10.2	>0.05	64.6 ± 10.7	65.9 ± 11	61.3 ± 10	>0.05
Height (cm)[a]	163 ± 8	162 ± 7	163 ± 8	>0.05	162 ± 8	163 ± 7	160 ± 7	>0.05
Body mass index (kg/cm^2)[a]	25 ± 3	25 ± 3	25 ± 3	>0.05	25 ± 3	25 ± 3	24 ± 3	>0.05
Radiation dose								
Volume CT dose index (mGy)[a]	10.7 ± 1.5	11.1 ± 0.8	11.2 ± 0.7	>0.05	9.2 ± 1.6	9 ± 5.3	9 ± 0.5	>0.05
Dose-length product (mGy-cm)[a]	444 ± 120	456 ± 58	484 ± 46	>0.05	371 ± 75	375 ± 20	380 ± 19	>0.05

Note.-Data in parentheses are percentages.
[a] **Data are mean ± standard deviation.**

deviation and were analyzed using One-Way ANOVA. Continuous variables with severely skewed distribution were shown as median (interquartile range) and the data were compared using the Wilcoxon rank sum test. Qualitative variables were described using frequency (percentage) and compared by chi-square test. Reader agreement for the assessment of subjective image quality was evaluated by Kappa test. $P < 0.05$ was considered statistically significant.

3. Results

3.1. Study participants

The basic profile of the three groups is shown in Table 2. There was no statistical difference in age, height, weight, body mass index, gender distribution among the three groups both in single energy mode and dual energy mode (all $p > 0.05$).

3.2. Objective image quality

Table 3 summarizes the CT values for the superior sagittal sinus, great cerebral vein, sigmoid sinus, aortic arch, ICA, MCA, SNR and CNR for ICA, and MCA for the three sets of images acquired using single-energy or dual-energy mode scans. The CT values of the superior sagittal sinus, great cerebral vein, and sigmoid sinus in ascending aorta group were all significantly lower than those in descending aorta group (in single energy mode: 223 HU vs 152 HU, 179 HU vs 123 HU, 142 HU vs 96 HU, respectively, all $p < 0.001$; in dual energy mode: 199 HU vs 146 HU, 166 HU vs 113 HU, 129 HU vs 94 HU, respectively, all $p < 0.001$). No significant differences for venous CT values were found between the ascending aorta group and aortic arch group. In addition, no significant differences were found in the CT values, SNR and CNR of ICA and MCA among the three groups ($p > 0.05$). Fig. 4 shows CTA images in the descending aorta group (Fig. 4A), aortic arch group (Fig. 4B), and ascending aorta group (Fig. 4C), respectively.

3.3. Subjective image quality

Reader agreement for the assessment of subjective image quality was high (kappa = 0.91). Significant differences were observed in subjective image quality among the three groups (Fig. 5). The number of images with grade 4 was 37 in the ascending aorta group which was significant higher than those in aortic arch group and descending aorta group ($p < 0.001$). In addition, the number of images with grade 1 in descending aorta group was significantly larger than that in ascending aorta group (17.7% vs 1.1%, $p < 0.01$) (Fig. 5).

3.4. Retrospective analysis for monitoring images

We retrospectively measured the CT values of the monitoring images in ascending aorta group and descending aorta group. The trigger threshold was firstly reached in ascending aorta in 64 cases in the ascending aorta group and in 66 cases in descending aorta group. The rest cases reached the trigger threshold at the same time. A case that firstly reached the trigger threshold in ascending aorta is shown in Fig. 6 (A-E).

4. Discussion

The bolus tracking technique has been widely used in CTA. For cervicocerebral CTA, ROI has been placed in the ascending aorta, the aortic arch, and the descending aorta. In this study, we compared the imaging quality of cervicocerebral CTA when the ROI was placed in various positions. Our data showed that the arterial CT values were greater than 250 HU regardless of ROI positions which

Table 3
Objective image quality.

	Single-Energy				Dual-Energy			
Variables	Ascending aorta	Aortic arch	Descending aorta	*P*	Ascending aorta	Aortic arch	Descending aorta	*P*
Superior sagittal sinus[a]	152 ± 48	165 ± 46	223 ± 56	<0.001	146 ± 40	159 ± 39	199 ± 51	<0.001
Great cerebral vein[a]	123 ± 39	133 ± 35	179 ± 45	<0.001	113 ± 37	127 ± 34	166 ± 47	<0.001
Ethmoid sinus[a]	96 ± 29	109 ± 31	142 ± 44	<0.001	94 ± 22	106 ± 29	129 ± 36	<0.001
Aortic arch[a]	347 ± 49	366 ± 50	359 ± 67	>0.05	346 ± 47	357 ± 60	379 ± 59	>0.05
ICA								
CT value[a]	343 ± 54	366 ± 60	357 ± 78	>0.05	346 ± 49	337 ± 64	381 ± 58	>0.05
SNR[a]	61 ± 22	64 ± 17	60 ± 21	>0.05	60 ± 21	57 ± 19	57 ± 14	>0.05
CNR[a]	50 ± 20	53 ± 16	49 ± 21	>0.05	49 ± 18	56 ± 13	48 ± 12	>0.05
MCA								
CT value[a]	309 ± 52	309 ± 50	311 ± 63	>0.05	317 ± 47	292 ± 56	330 ± 52	>0.05
SNR[a]	38 ± 9	35 ± 7	39 ± 11	>0.05	35 ± 7	36 ± 6	35 ± 7	>0.05
CNR[a]	34 ± 9	31 ± 7	35 ± 11	>0.05	32 ± 7	32 ± 5	32 ± 7	>0.05

[a] **Data are mean ± standard deviation.**

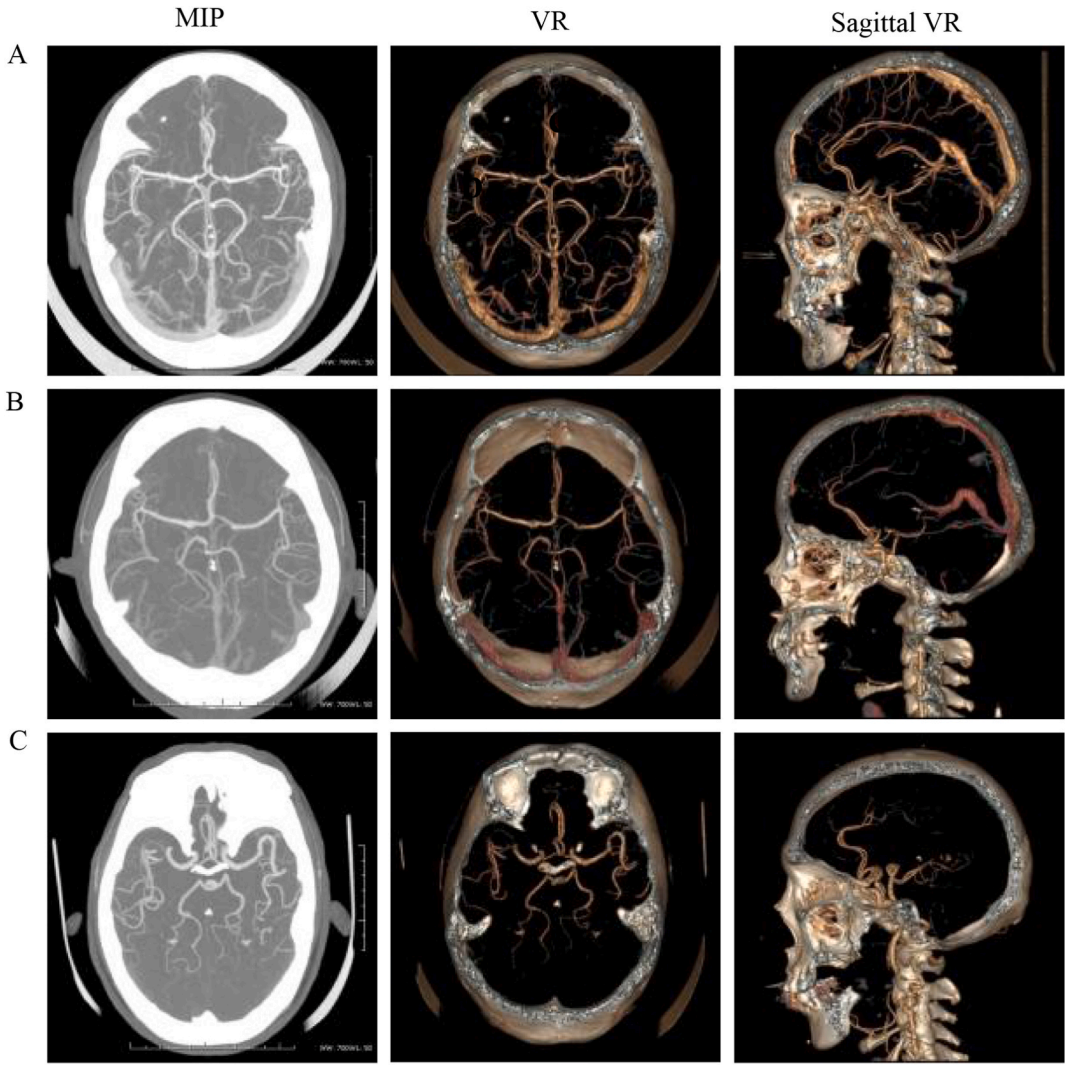

Fig. 4. Computed tomography agiography images in descending aorta group (A), aortic arch group (B) and ascending aorta group (C), respectively. A: A 67-year-old woman, maximum intensity projection (MIP), volume rendering (VR) and sagittal VR both showed venous noise. B: A 46-year-old woman, MIP, VR and sagittal VR showed moderate venous noise. C: A 69-year-old man, no obvious venous noise was observed.

satisfied the diagnostic requirements [17,18]. No significant differences were observed in SNR and CNR among the three groups. However, placing ROIs in the ascending aorta significantly affected the display of venous structure.

It is widely known that bolus tracking technology required an additional delay after the ROI has reached the trigger threshold before the scan can begin [1–4]. The additional lag time depends on the device's parameter settings and the speed at which the scanning bed is moved. Previous studies have reported an additional delay ranging from 2 to 8 s [19–22]. This is a crucial factor for venous structure imaging [23,24]. It is still a challenge to obtain an optimal scan timing.

When the bolus tracking technique was used for cervicocerebral CTA in clinical practice, we observed variations in ROI placement [12–14]. ROI sites placed in the ascending aorta, the aortic arch and the descending aorta are all used. The ACR guideline also recommended monitoring aorta as the vessel of interest [15]. From an anatomical and blood circulation perspective, the ascending aorta is enhanced before the other two monitoring levels. When a uniform trigger threshold is set, the ascending aorta may initiate the scan earlier than the other two monitoring levels, potentially leading to a shorter additional delay time. This has the potential to reduce likelihood of venous structure imaging. The significance of interpreting venous structure on CTA has not been clarified. However, the recent ACR guideline shows that evaluation of images for venous pathology is also necessary, even although venous structures are adequately opacified on CTA images [15]. Our data suggested that the ROI should be placed in the descending aorta, taking into consideration to both arterial and venous structures. If the arteries have priority, the ROI should be placed in the ascending aorta. Monitoring the descending aorta is also robust because it is situated away from the superior vena cava and experience minimal movement caused by the heart beat. The risk of sclerotic bundle artifacts from the superior vena cava and arterial displacement due to cardiac pulsation is very low. Our study showed that those artifacts only slightly increased the CT values of the ascending aorta.

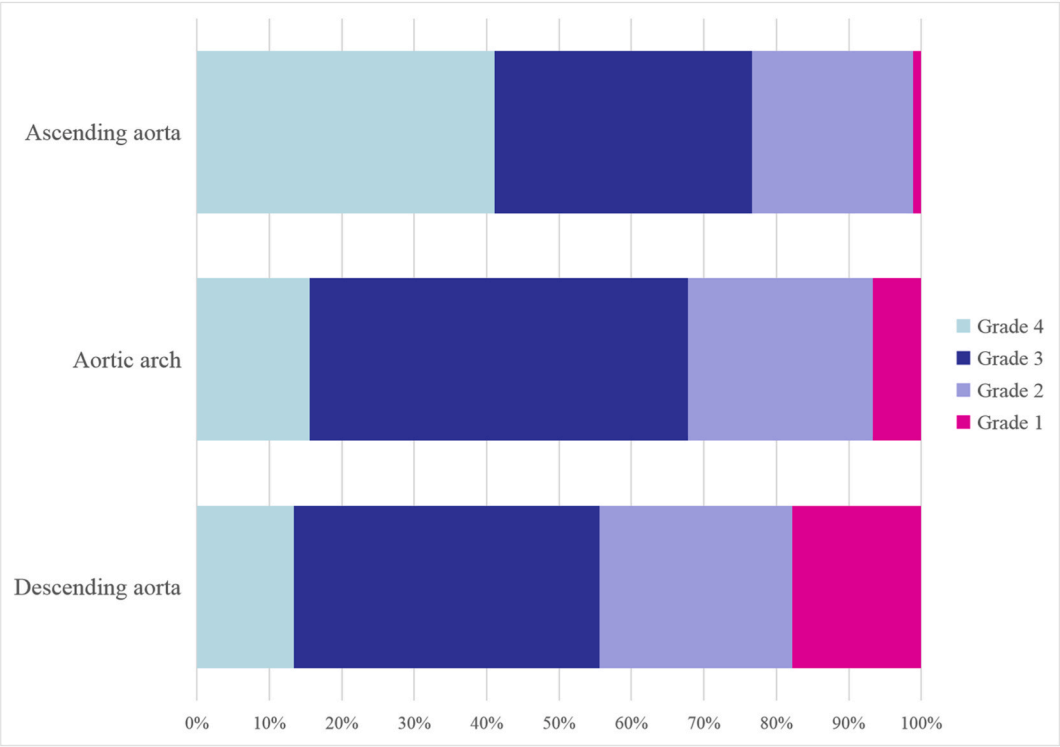

Fig. 5. Subjective evaluation of images quality. The images were divided into four grades.

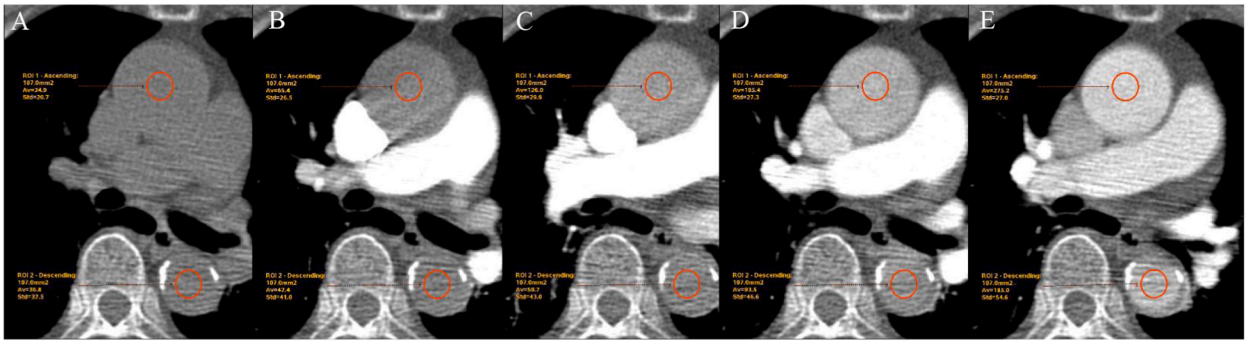

Fig. 6. Retrospective analysis of monitoring images in a 74-year-old women underwent single energy scan. (A) The monitoring of tracheal bifurcation levels at the 8 s after the contrast injection. The ascending aortic region of interest (ROI) had a background computed tomography (CT) value of 34.8 hounsfield unit (HU) and the descending aortic ROI had a background CT value of 34.9 HU; (B–C) The contrast agent circulated from the superior vena cava to the pulmonary artery; (D) The CT values in ascending aortic ROI was 195.1 HU, which firstly reached the trigger threshold (CT value $>$ 100), while the CT values in descending aortic ROI was 91.5 HU, which did not reached the trigger threshold. (E) The CT values ascending aortic ROI was 272.2 HU and was 188.1 HU in the descending aortic ROI after a 2 s blood circulation (monitoring sequence with a 1 s exposure time and 1 s interval every 2 s). If monitoring ROI was placed in the ascending aorta, the scan could been triggered 2 s earlier.

Although the CT value has increased, it has still not reached the threshold. Our data showed that there were no false triggers in the ascending aorta group. The risk of false trigger was very low even though the ROI was placed in the ascending aorta. Huang et al. [25] showed that the placement of in the descending aorta reduces the chance of suboptimal intracranial CTA. However, no significant differences were found in our analysis. Scanning was triggered without delay when the CT attenuation measurement of the ROIs reached 60 Hounsfield Unit (HU) above baseline measurement in Huang's study. Our study selected a higher threshold and 2.2 s delay time. Another reason is for the venous streak or beam hardening artifacts which will caused false trigger. False trigger would cause poor image quality.

Monitoring images from both the ascending and descending aorta groups were retrospectively analyzed in our study. The ascending aorta firstly reached the trigger threshold was observed in 73% cases in the descending aorta group. For those cases the scan time may

be delayed, which could result in additional venous structure imaging. The image with grade 1–2 was mainly observed in such cases in the descending aorta group. The venous structure imaging in those cases would have been affected if ascending aorta monitoring had been chosen because the scan timing was 2 s earlier (monitoring sequence of scans every 2 s with 1 s exposure time and 1 s interval). In addition, the ascending aorta firstly reached the trigger threshold in 71% of the cases in the ascending aorta group, and the majority of cases had image with grade 3–4, demonstrating the loss of venous structure imaging in monitoring the ascending aorta.

Many researchers employ low-tube voltage scanning protocols, which cause variable ROI trigger thresholds ranging from 80 to 175 HU [18–20,26]. Lowering the tube voltage and keV energy level significantly improves the CT value of enhanced vessels [27–29], and the threshold can directly affect the triggering timing. Our study established an ROI trigger threshold of 100 HU for the single-energy mode with tube voltage of 120 kVp and an ROI trigger threshold of 100HU for the dual-energy mode [30–32].

The 256-row Revolution CT was used in our study, which offered two scanning mode: single energy mode and dual energy mode. The dual energy mode has some special role, such as virtual monoenergetic imaging (VMI) and VMI plus [33,34]. These technique are helpful for artifact reduction, displaying of calcified plaques (32), and salvaging examinations with poor contrast attenuation [35]. Dual energy mode was also used for some patients with dentures because metal artifact reduction can be performed in this mode. However, we did not extensively compare the intracranial image quality between single energy mode and dual energy mode because our study focused on the effects of ROI positions on image quality. Our results indicated that the venous structure imaging was poor, while the arterial vessels imaging was similar when ROI was placed in ascending aorta compared to when ROI was placed in the descending aorta both in single energy mode and dual energy mode.

The limitations of our study must be acknowledged. Firstly, the diagnostic performance of the three approaches was not evaluated, and the CT values are not always representative of diagnostic performance. Second, we used a high-end CT with a detector width of 16 cm. Whether our approaches can be applied to other CT scanners needs to be confirmed. Third, the ASiR-V iterative reconstruction software chose a grade of 70% and no other grades were attempted, which may affect image quality, as well as SNR and CNR values. Fourth, only subjects weighing less than 100 kg were included in this study, and the contrast injection protocol should be adjusted for subjects >100 kg.

In conclusion, the positioning of ROI for cervicocerebral CTA did not affect the arterial image quality. However, venous structures imaging was affected when the ROI was placed in the ascending aorta using bolus tracking technology. Monitoring the ascending aorta during cervicocerebral CTA reduces imaging ability of intracranial venous structure.

Ethics statement

This study was approved the Institutional Review Board of Affiliated Hospital of Nanjing University of Chinese Medicine (2021NL-157-01).

Funding statement

This study was funded by Developing Program for High-level Academic Talent in Jiangsu Provincial Hospital of Chinese Medicine (Y21050, Y2021rc03).

Availability of data and materials

The datasets generated and/or analyzed during the current study are available from the Corresponding author on reasonable request.

Additional information

No additional information is available for this paper.

CRediT authorship contribution statement

Huiming Wu: Writing – review & editing, Writing – original draft, Formal analysis, Data curation, Conceptualization. **Jianhua Wang:** Writing – original draft, Formal analysis, Data curation. **Maodong Zhou:** Writing – original draft, Formal analysis, Data curation. **Yajie Wang:** Writing – original draft, Formal analysis, Data curation. **Can Cui:** Formal analysis, Data curation. **Changsheng Zhou:** Writing – original draft, Formal analysis, Data curation. **Xiao Chen:** Writing – review & editing, Writing – original draft, Formal analysis, Conceptualization. **Zhongqiu Wang:** Writing – review & editing, Funding acquisition, Formal analysis.

Declaration of competing interest

The authors declare that they have no known competing financial interests or personal relationships that could have appeared to influence the work reported in this paper.

Acknowledgement

None.

References

[1] R. Hinzpeter, M. Eberhard, R. Gutjahr, et al., CT angiography of the aorta: contrast timing by using a fixed versus a patient-specific trigger delay, Radiology 291 (2) (2019) 531–538, https://doi.org/10.1148/radiol.2019182223.
[2] M.M. Lell, K. Anders, M. Uder, et al., New techniques in CT angiography, Radiographics 26 (Suppl 1) (2006) S45–S62, https://doi.org/10.1148/rg.26si065508.
[3] J.J. Kim, W.P. Dillon, C.M. Glastonbury, J.M. Provenzale, M. Wintermark, Sixty-four-section multidetector CT angiography of carotid arteries: a systematic analysis of image quality and artifacts, AJNR Am J Neuroradiol 31 (1) (2010) 91–99, https://doi.org/10.3174/ajnr.A1768.
[4] H. Wu, X. Chen, H. Zhou, et al., An optimized test bolus for computed tomography pulmonary angiography and its application at 80 kV with 10 ml contrast agent, Sci. Rep. 10 (1) (2020) 10208, https://doi.org/10.1038/s41598-020-67145-9.
[5] J.L. Brisman, J.K. Song, D.W. Newell, Cerebral aneurysms, N. Engl. J. Med. 355 (9) (2006) 928–939, https://doi.org/10.1056/NEJMra052760.
[6] S.J. Kim, R.G. Nogueira, D.C. Haussen, Current understanding and gaps in research of carotid webs in ischemic strokes: a review, JAMA Neurol. 76 (3) (2019) 355–361, https://doi.org/10.1001/jamaneurol.2018.3366.
[7] W.J. Powers, A.A. Rabinstein, T. Ackerson, et al., Guidelines for the Early Management of Patients With Acute Ischemic Stroke: 2019 Update to the 2018 Guidelines for the Early Management of Acute Ischemic Stroke: a Guideline for Healthcare Professionals From the American Heart Association/American Stroke Association [published correction appears in Stroke. 2019;50(12):e440-e441], Stroke 50 (12) (2019) e344–e418, https://doi.org/10.1161/STR.0000000000000211.
[8] D. Millon, A.L. Derelle, P. Omoumi, et al., Nontraumatic subarachnoid hemorrhage management: evaluation with reduced iodine volume at CT angiography, Radiology 264 (1) (2012) 203–209, https://doi.org/10.1148/radiol.12111384.
[9] T. Shirasaka, A. Hiwatashi, K. Yamashita, et al., Optimal scan timing for artery-vein separation at whole-brain CT angiography using a 320-row MDCT volume scanner, Br. J. Radiol. 90 (1070) (2017) 20160634, https://doi.org/10.1259/bjr.20160634.
[10] N. Takeyama, K. Kuroki, T. Hayashi, et al., Cerebral CT angiography using a small volume of concentrated contrast material with a test injection method: optimal scan delay for quantitative and qualitative performance, Br. J. Radiol. 85 (1017) (2012) e748–e755, https://doi.org/10.1259/bjr/31882420.
[11] K. Das, S. Biswas, S. Roughley, M. Bhojak, S. Niven, 3D CT cerebral angiography technique using a 320-detector machine with a time-density curve and low contrast medium volume: comparison with fixed time delay technique, Clin. Radiol. 69 (3) (2014) e129–e135, https://doi.org/10.1016/j.crad.2013.10.021.
[12] M. Mannil, J. Ramachandran, I. Vittoria de Martini, et al., Modified dual-energy algorithm for calcified plaque removal: evaluation in carotid computed tomography angiography and comparison with digital subtraction angiography, Invest. Radiol. 52 (11) (2017) 680–685, https://doi.org/10.1097/RLI.0000000000000391.
[13] Caton M Jr Travis, N. Miskin, J.P. Guenette, The role of computed tomography angiography as initial imaging tool for acute hemorrhage in the head and neck, Emerg. Radiol. 28 (2) (2021) 215–221, https://doi.org/10.1007/s10140-020-01835-9.
[14] V. Neuhaus, N. Große Hokamp, N. Abdullayev, et al., Comparison of virtual monoenergetic and polyenergetic images reconstructed from dual-layer detector CT angiography of the head and neck, Eur. Radiol. 28 (3) (2018) 1102–1110, https://doi.org/10.1007/s00330-017-5081-8.
[15] ACR–ASNR–SPR PRACTICE PARAMETER FOR THE PERFORMANCE AND INTERPRETATION OF CERVICOCEREBRAL COMPUTED TOMOGRAPHY ANGIOGRAPHY, CTA), 2020. https://www.acr.org/-/media/ACR/Files/Practice-Parameters/CervicoCerebralCTA.pdf.
[16] Q. Wu, D. Shi, T. Cheng, et al., Improved display of cervical intervertebral discs on water (iodine) images: incidental findings from single-source dual-energy CT angiography of head and neck arteries, Eur. Radiol. 29 (1) (2019) 153–160, https://doi.org/10.1007/s00330-018-5603-z.
[17] A. Waaijer, M. Prokop, B.K. Velthuis, C.J. Bakker, G.A. de Kort, M.S. van Leeuwen, Circle of Willis at CT angiography: dose reduction and image quality–reducing, Radiology 242 (3) (2007) 832–839, https://doi.org/10.1148/radiol.2423051191.
[18] E.S. Cho, T.S. Chung, S.J. Ahn, K. Chong, J.H. Baek, S.H. Suh, Cerebral computed tomography angiography using a 70 kVp protocol: improved vascular enhancement with a, Eur. Radiol. 25 (5) (2015) 1421–1430, https://doi.org/10.1007/s00330-014-3540-z.
[19] Y. Chen, X. Zhang, H. Xue, et al., Head and neck angiography at 70 kVp with a third-generation dual-source CT system in patients: comparison with 100 kVp, Neuroradiology 59 (11) (2017) 1071–1081, https://doi.org/10.1007/s00234-017-1901-4.
[20] Q. Wu, D. Shi, T. Cheng, et al., Improved display of cervical intervertebral discs on water (iodine) images: incidental findings from single-source dual-energy CT angiography of head and neck arteries, Eur. Radiol. 29 (1) (2019) 153–160, https://doi.org/10.1007/s00330-018-5603-z.
[21] L. Schimmöller, R.S. Lanzman, P. Heusch, et al., Impact of organ-specific dose reduction on the image quality of head and neck CT angiography, Eur. Radiol. 23 (6) (2013) 1503–1509, https://doi.org/10.1007/s00330-012-2750-5.
[22] D. Wang, Z. Li, X. Zheng, et al., Head and neck CT angiography to assess the internal carotid artery stealing pathway, BMC Neurol. 20 (1) (2020) 334, https://doi.org/10.1186/s12883-020-01915-w.
[23] M. Wang, W. Li, D. Lun-Hou, J. Li, R. Zhai, Optimizing computed tomography pulmonary angiography using right atrium bolus monitoring combined with spontaneous respiration, Eur. Radiol. 25 (9) (2015) 2541–2546, https://doi.org/10.1007/s00330-015-3664-9.
[24] K.T. Bae, Test-bolus versus bolus-tracking techniques for CT angiographic timing, Radiology 236 (1) (2005) 369–370, https://doi.org/10.1148/radiol.2361050123.
[25] R.Y. Huang, B.B. Chai, T.C. Lee, Effect of region-of-interest placement in bolus tracking cerebral computed tomography angiography, Neuroradiology 55 (10) (2013 Oct) 1183–1188, https://doi.org/10.1007/s00234-013-1228-8.
[26] D. Zopfs, S. Lennartz, N. Abdullayev, et al., Generally applicable window settings of low-keV virtual monoenergetic reconstructions in dual-layer CT-angiography of the head and neck, Quant. Imag. Med. Surg. 11 (8) (2021) 3408–3417, https://doi.org/10.21037/qims-20-1140.
[27] G.Z. Chen, L.J. Zhang, U.J. Schoepf, et al., Radiation dose and image quality of 70 kVp cerebral CT angiography with optimized sinogram-affirmed iterative reconstruction: comparison with 120 kVp cerebral CT angiography, Eur. Radiol. 25 (5) (2015) 1453–1463, https://doi.org/10.1007/s00330-014-3533-y.
[28] T. Emrich, J. O'Doherty, U.J. Schoepf, et al., Reduced iodinated contrast media administration in coronary CT angiography on a clinical photon-counting detector CT system: a phantom study using a dynamic circulation model, Invest. Radiol. 58 (2) (2023) 148–155, https://doi.org/10.1097/RLI.0000000000000911.
[29] M.H. Albrecht, T.J. Vogl, S.S. Martin, et al., Review of clinical applications for virtual monoenergetic dual-energy CT, Radiology 293 (2) (2019) 260–271, https://doi.org/10.3390/jcm12247766.
[30] Y. Noda, F. Nakamura, N. Kawai, et al., Optimized bolus threshold for dual-energy CT angiography with monoenergetic images: a randomized clinical trial, Radiology 300 (3) (2021) 615–623, https://doi.org/10.1148/radiol.2021210102.
[31] M. Beeres, J. Trommer, C. Frellesen, et al., Evaluation of different keV-settings in dual-energy CT angiography of the aorta using advanced image-based virtual monoenergetic imaging, Int. J. Cardiovasc. Imag. 32 (1) (2016) 137–144, https://doi.org/10.1007/s10554-015-0728-5.
[32] D.F. Pinho, N.M. Kulkarni, A. Krishnaraj, S.P. Kalva, D.V. Sahani, Initial experience with single-source dual-energy CT abdominal angiography and comparison with single-energy CT angiography: image quality, enhancement, diagnosis and radiation dose, Eur. Radiol. 23 (2) (2013) 351–359, https://doi.org/10.1007/s00330-012-2624-x.

[33] T. D'Angelo, S. Mazziotti, G. Ascenti, J.L. Wichmann, Miscellaneous and emerging applications of dual-energy computed tomography for the evaluation of pathologies in the head and neck, Neuroimaging Clin. 27 (3) (2017) 469–482, https://doi.org/10.1016/j.nic.2017.04.008.
[34] T. D'Angelo, L.R.M. Lanzafame, A. Micari, A. Blandino, et al., Improved coronary artery visualization using virtual monoenergetic imaging from dual-layer spectral detector CT angiography, Diagnostics 13 (16) (2023) 2675, https://doi.org/10.3390/diagnostics13162675.
[35] M.H. Albrecht, T.J. Vogl, S.S. Martin, et al., Review of clinical applications for virtual monoenergetic dual-energy CT, Radiology 293 (2) (2019) 260–271, https://doi.org/10.1148/radiol.2019182297.